

MOLECULAR ABUNDANCES IN CRL 618

JUAN R. PARDO AND JOSÉ CERNICHARO

Departamento de Astrofísica Molecular e Infrarroja, Instituto de Estructura de la Materia CSIC,
Madrid, Spain; pardo@damir.iem.csic.es, cerni@damir.iem.csic.es

Received 2006 May 23; accepted 2006 September 7

ABSTRACT

In previous works we have modeled the different gas regions of the proto–planetary nebula CRL 618 by studying the large number of lines from the cyanopolyynes detected in a millimeter-wave line survey of this object. In this work we retrieve the rotational temperatures (T_r) and abundance ratios R with respect to HC_3N (used as reference) for all molecular species detected in the survey by running grids of models in the (R, T_r) space to find the minimum of a weighted χ^2 defined for this analysis. This provides the best knowledge to date of the (polar) molecular composition of CRL 618 thanks to the uniform calibration of the whole survey and the large number of lines available from each species, allowing comparisons with predictions made by chemical models of C-rich post-AGB objects. A significantly lower value of the $^{12}\text{C}/^{13}\text{C}$ ratio has been revealed in the gas closest to central star with respect to the colder and outer envelope. It can be due to ^{13}C -rich material, produced in a late CNO cycling occurred in the central star, being currently injected into this inner gas envelope.

Subject headings: circumstellar matter — ISM: molecules — radio lines: stars — stars: AGB and post-AGB — stars: carbon — stars: individual (CRL 618)

Online material: color figures

1. INTRODUCTION

In CRL 618 and other post-AGB objects, small hydrocarbons and pure carbon chains are thought to be the small bricks from which larger C-rich molecules can be built, those widely acknowledged as the carriers of the unidentified infrared bands (UIBs; see a recent review in Williams 2003). The complete millimeter-wave line survey of CRL 618 performed by us with the IRAM 30 m telescope in the frequency range 80–276 GHz allows us to determine the chemical abundances of these and other detected molecular species with a high degree of accuracy, which in turn benefits the validation and improvement of chemical models (see Cernicharo [2004] for the CRL 618 case). This is possible due to the large number of lines (more than 20 for some species) that are available with a quite uniform calibration. For this task, we can also take advantage of the detailed study of the physical conditions in the different gas regions of CRL 618 already performed using the lines of the cyanopolyynes and the knowledge of the spectral characteristics of the continuum flux in the surveyed frequency range (Pardo et al. 2004, 2005, hereafter P04 and P05, respectively). Once the best fit for the different species is obtained, a whole model can be run that will help in the task of reducing the number of unidentified features.

We need to establish a strategy to compare data and model in order to retrieve the parameters for which both are closer in an unbiased way. Direct χ^2 fitting algorithms are difficult to apply due to the large number of lines to consider for each species, their possible blending with lines from other species, and the large number of model parameters (see P04, P05). Therefore, we need an adapted approach, and this is described in § 3. Results are presented and discussed in § 4, where the molecular species have been divided in groups according to criteria such as chemical properties and their location in the different gas regions of CRL 618. Finally, § 5 summarizes this work.

2. OBSERVATIONS

The IRAM 30 m observations were described in detail in the previous P04 and P05 papers. Since the regions from which both

the line emission and the continuum are arising are always much smaller than the beam, the nominal values provided in the IRAM Web page were used for T_A^* to T_{MB} or flux conversions (see P04). By looking at contiguous HC_3N and HC_5N $v = 0$ lines, it appears that calibration inconsistencies larger than 15% are rare. Even if a spectrum is affected by a large absolute error, there is little impact on our analysis, because it is made in terms of the line-to-continuum ratio, once the latter was characterized as an average for the period 1994–2002 in P04 (see below). For further details on the IRAM 30 m observations, see the above references. These data are being complemented with observations carried out with the Caltech Submillimeter Observatory (CSO) making use of a helium-cooled SIS receiver operating in double-sideband mode in the range 280–360 GHz. The pointing was checked on the available planets and kept within $3''$ – $4''$ accuracy. The back end is an acousto-optical spectrometer (AOS) with a frequency coverage that exceeds the useful instantaneous bandwidth of the receiver (~ 0.95 GHz) and provides ~ 1 MHz resolution. Typical system temperatures have been 400–1200 K.

3. ANALYSIS

3.1. Reference Model

A model has been developed to study the lines of cyanopolyne species arising from the slowly expanding gas envelope (SEE; P04) and the cold circumstellar shell (CCS; P05) in CRL 618. As in those references, the analysis assumes local thermodynamic equilibrium (LTE). The physical parameters of the model can be found in Figure 4 and Table 3 of P04 and in Figure 3 and Table 2 of P05. Those values are kept unchanged for the analysis in this work with the exception of the rotational temperature and the inverse abundance ratio $[\text{HC}_3\text{N}]/[\text{X}]$ (R_X) for the different molecular species, which are determined from the data. Because we provide our results in terms of R_X , it is necessary to keep in mind the HC_3N column densities in the reference P04/P05 model for different impact parameters (see Table 1). Because the inclination of the line of sight breaks the symmetry of the problem with respect to the position angle in the plane of the sky, the

TABLE 1
REFERENCE VALUES OF HC_3N COLUMN DENSITIES
IN THE CRL 618 MODEL USED IN THIS WORK

Impact Parameter	Equivalent Diameter (arcsec)	$\int[\text{HC}_3\text{N}] ds$ (cm^{-2})	Fraction from CCS
0.00–0.06.....	0.0–0.27	3.01×10^{17}	<0.01
0.09.....	0.41	5.53×10^{17}	0.02
0.15.....	0.68	2.94×10^{17}	0.03
0.21.....	0.95	1.89×10^{17}	0.05
0.27.....	1.22	1.78×10^{17}	0.06
0.33.....	1.48	1.40×10^{17}	0.08
0.39.....	1.76	1.17×10^{17}	0.09
0.45.....	2.02	7.01×10^{16}	0.16
0.51.....	2.31	3.93×10^{16}	0.32
0.57.....	2.56	2.50×10^{16}	0.57
0.63.....	2.84	1.79×10^{16}	1.00
0.69.....	3.11	2.45×10^{16}	1.00
0.75.....	3.38	2.30×10^{16}	1.00
0.81.....	3.65	2.03×10^{16}	1.00
0.87.....	3.92	1.62×10^{16}	1.00
0.93.....	4.19	1.20×10^{16}	1.00
0.99.....	4.47	5.15×10^{15}	1.00

NOTES.—The first line gives the average column density in front of the continuum source. The fourth column gives the fraction of gas from the CCS in the total column density.

column densities that we provide in that table for each impact parameter are averaged with respect to that angle. The impact parameter p is defined as the ratio of the angular distance to the central object divided by the outer radius of the CCS (2.25"). With this reference, the continuum source ends at $p = 0.06$ (total diameter of 0.27"; see Table 2 of P04), the SEE ends at $p = 1/3$ (long axis of 1.5"), and the CCS extends from $p = 2/3$ to 1.0 (3"–4.5" diameter). The high-velocity wind (HVW) is included as in P05. The CCS should be considered more extended for very abundant molecules such as CO, HCN, HNC, and HCO^+ , as we see in § 4.3.

3.2. Method

Most of the emission from the species analyzed in this work originates in the CCS of CRL 618, as revealed by the much lower ratio between absorption and emission in the line profiles at ~ 3 mm wavelength with respect to rotational lines in vibrationally excited states of HC_3N that mostly originate in the inner SEE (P04; Wyrowski et al. 2003). Therefore, in this work we mainly focus on the CCS (exceptions can be found in § 4.2). In order to determine $R_{X, \text{CCS}}$ and $T_{r, X, \text{CCS}}$ for a given species X, we first select for the analysis a set of lines belonging to it from the line survey according to the following criteria.

1. Blending with species other than $\text{HC}_{3,5,7}\text{N}$ does not exist. We can tolerate small blendings with $\text{HC}_{3,5,7}\text{N}$ lines, since those lines are reproduced according to P04 and P05.
2. The lines are well spaced in the frequency range of the survey.
3. The energy levels involved represent well the total energy range covered in the survey for the concerned molecule.

For the N lines selected for species X, we define the observed area $A_{i, \text{obs}}$ and the simulated area $A_{i, \text{sim}}$ by adding the absolute values of the absorption and the emission parts of the P Cygni profile. Of course, this means that we are assuming that the line shape is determined by the morphology and dynamics for the SEE and CCS determined in P04 and P05, which is a reasonably

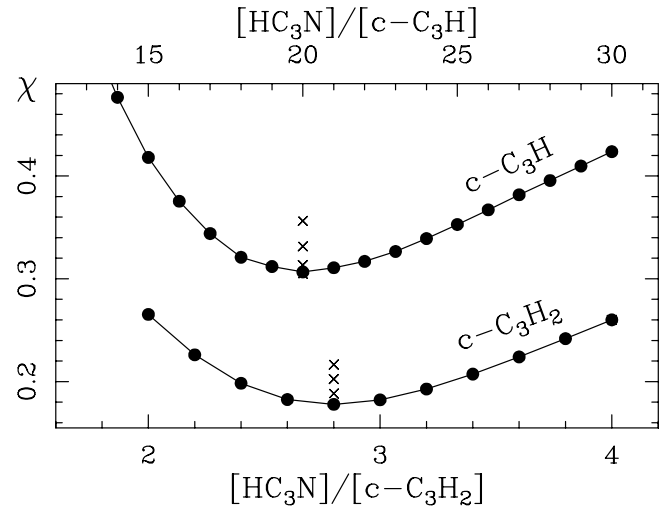


FIG. 1.—Parameter χ , as defined in eq. (1), for a grid of models run to fit the cyclic- C_3H_2 and cyclic- C_3H lines shown in Fig. 3. In the $\text{c-C}_3\text{H}_2$, curve the rotational temperature in the CCS is 27.5 K, the one that provides the lowest χ for a ratio $[\text{HC}_3\text{N}]/[\text{c-C}_3\text{H}_2]$ equal to 2.8. The associated crosses indicate the value of χ for that abundance ratio and slightly higher rotational temperatures: 30.0, 32.5, and 35.0 K. The other dots and crosses correspond to the $\text{c-C}_3\text{H}$ analysis, but in this case the best-fit rotational temperature is 30.0 K, and the crosses correspond to calculations for 32.5, 35.0, and 37.5 K. For temperatures below the one associated with the curves shown, χ rises again, although these points are not plotted so as to avoid confusion in the figure.

good hypothesis if we have a look at Figures 2–7. Then, we define the χ^2 parameter for a given simulation

$$\chi^2 = \frac{1}{N} \sum_{i=1}^N \left(\frac{A_{i, \text{sim}} - A_{i, \text{obs}}}{A_{i, \text{obs}}} \right)^2 \quad (1)$$

in order to find a minimum of it by running an array of models for the CCS in which $R_{X, \text{CCS}}$ and $T_{r, X, \text{CCS}}$ vary. As a first step, we

TABLE 2
MOLECULAR ABUNDANCES AND ASSOCIATED ROTATIONAL TEMPERATURES

Species	Figure	R_{CCS}	T_{CCS}	χ_{min}
c- C_3H_2	3	2.8	27.5	0.178
c- C_3H	3	20.0	30.0	0.307
H_2CO	2	8.0	30.0	0.351
H_2^{13}CO	>300	30.0	...
CS.....	2	8.0	30.0	0.222
SiO.....	2	80.0	25.0	0.123
C_3N	4	8.5	30.0	0.069
C_4H	4	1.0	30.0	0.123
l- C_3H	4	60.0	25.0	0.424
C_5H	4	200.0	30.0	...
N_2H^+	40.0	30.0	Only 1 line
HCCNC.....	5	40.0	30.0	0.140
MgNC.....	5	10.0	30.0	0.288
CN.....	4	0.33	30.0	0.358
^{13}CN	15	30.0	...
CCH.....	4	2.0	30.0	0.385
^{13}CCH	≥ 80.0	30.0	...
C^{13}CH	≥ 80.0	30.0	...

NOTES.—Values are retrieved according to the method defined in § 3, for those molecules of CRL 618 that the data reveal to be present almost exclusively in the CCS. The quality of the retrieval can be evaluated by looking at the minimum χ , as defined in eq. (1) in this two-variable analysis. The error bars on the derived temperatures and abundance ratios do not exceed 10% (see § 3.2).

TABLE 3
ABUNDANCES OF SOME MOLECULAR SPECIES IN CRL 618

Species	Figure	R_{SEE}	R_{HVV}	R_{CCS}	D_{ext} (arcsec)	χ_{min}
CH ₃ CN.....	6	15.0	10.0	30.0	4.5	0.197
CH ₃ CCH.....	6	1.0	0.5	5.0	4.5	0.260
¹² CO.....	7	...	0.0015	0.01	17.1	0.182
¹³ CO.....	7	0.4	...	0.4	17.1	0.302
C ¹⁷ O.....	7	3.5	...	3.5	17.1	0.301
C ¹⁸ O.....	7	5.0	...	5.0	17.1	0.143
HCN.....	7	0.5	0.5	0.67	6.75	0.189
H ¹³ CN.....	7	7.5	7.5	30.0	6.75	0.197
HNC.....	7	5.0	5.0	6.0	6.75	0.381
HN ¹³ C.....	7	75.0	100.0	225.0	6.75	0.335
HCO ⁺	7	10.0	5.0	10.0	6.75	0.191
H ¹³ CO ⁺	7	400.0	6.75	0.404

NOTES.—These are abundances that the data suggest are also present in the SEE (contrary to those in Table 2) and, in some cases, are also more extended than those in Table 2. Their analysis has required extra steps with respect to those species in Table 2, as explained in §§ 4.2 and 4.3. The quality of the fit is given by the parameter χ_{min} (see eq. [1]).

consider that the concerned molecule is not present in the inner SEE, and once the best value of R_{CCS} is found, we check what the difference in χ is when $R_{\text{SEE}} = R_{\text{CCS}}$ and $T_{r,\text{SEE}} = 263$ K, as in P04, in order to see whether or not an improvement is possible. In most cases no improvement is found, indicating that the concerned molecule is basically not present in the SEE or that its emission from that region hardly shows up in the final profile (see § 4.1).

The model calculations have been done using the following (linear) quadratures.

1. 50 steps in the impact parameter from the center of the central object to the outer boundary of the CCS.
2. 50 steps for each path perpendicular to the plane of the sky with length equal to the diameter of the CCS.
3. 18 steps for the position angle in the plane of the sky (necessary because the model is not symmetric with respect to that angle in general).
4. Equal velocity resolution to the data.
5. Minimum steps of 2.5 K in $T_{r,X,\text{CCS}}$.
6. Different steps in $R_{X,\text{CCS}}$, depending on the species.

With these values, the necessary grid of models for a molecule where 8–10 lines are analyzed can be computed in a few minutes, thus keeping the analysis feasible. Figure 1 illustrates the process

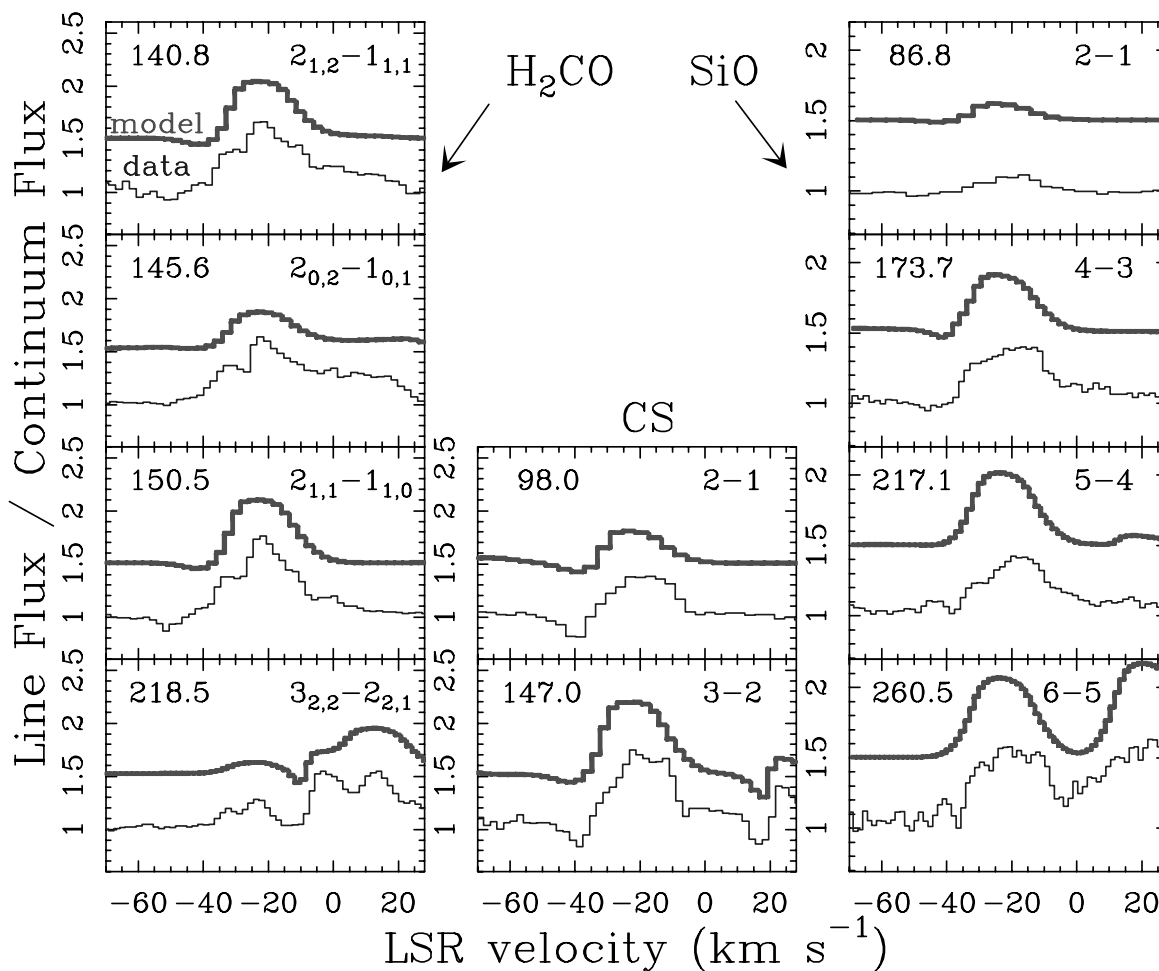


FIG. 2.—Data (not shifted) and best model (shifted by $0.5F_C$) for O-bearing molecules (other than the abundant CO and HCO⁺) and CS in CRL 618 (discussed in § 4.1.1). The rotational quantum numbers of the transitions and the central frequencies rounded to 0.1 GHz are indicated in each box. Extra features in the data correspond to vibrationally excited states of HC₃N (modeled according to P04) with the exception of two lines of c-C₃H₂ appearing at +18 km s⁻¹ in the 218.5 GHz spectrum and +20 km s⁻¹ in the 260.5 GHz spectrum. Because of lack of space, the extra features are not labeled in the figures. Nevertheless, there will be a complete line identification of the survey in an upcoming paper (J. R. Pardo et al. 2007, in preparation). [See the electronic edition of the Journal for a color version of this figure.]

for two molecules among those analyzed (see § 4.1.2). Numerically, we have established the error bars by looking at the range in the parameter under investigation for which $\Delta\chi/\chi_{\min}$ is within 5%. By looking at Figure 1, this is satisfied for $[\text{HC}_3\text{N}]/[\text{c-C}_3\text{H}]$ between 18 and 22, and for $[\text{HC}_3\text{N}]/[\text{c-C}_3\text{H}_2]$ between 2.5 and 3.1. In both cases, this is very close to $\pm 10\%$ with respect to the abundance ratios for which χ_{\min} is obtained. Of course, for a less abundant species, such as $\text{c-C}_3\text{H}$ in this Figure 1, the absolute error bar is larger than for $\text{c-C}_3\text{H}_2$, but in relative terms it is $\sim 10\%$. Similar results are obtained for the other species, and this is why we quote 10% as the uncertainty for the abundance ratios derived in this work. The best-fit temperatures found for all species in Table 2, are also within $\sim \pm 10\%$ of the average.

Finally, molecules such as CO appear to be more extended than the original CCS of P05 (see above). In other cases the line profiles show evidence of competing features from more than one gas region. For those cases we have approached a good reproduction of the line profiles in several steps, using complementary data such as the lines from isotopomers or vibrationally excited states, and/or extending the CCS size (for CO, HCN, ...). No grid of models could be properly evaluated in those cases due to the introduction of extra parameters (abundances in more than one region, angular extension of the emission for very abundant molecules) that make the dimension of the space to explore too large (§§ 4.2 and 4.3).

4. RESULTS AND DISCUSSION

We concentrate only on detected molecules in several transitions, so that useful constraints on their abundance and the physical parameters of CRL 618 can be obtained. In this object, there are other trace species that need a very long integration time for the detection of only one line. They are of course extremely interesting but will be, or have already been, discussed elsewhere.

For presenting and discussing the results, we find it useful to divide the analyzed molecules into different groups, related first with its location in CRL 618, and second to chemical properties. The main results are summarized in Tables 2 and 3.

4.1. Molecules Present Almost Exclusively in the CCS

The observational evidence in CRL 618 shows that the cyanopolyynes are very abundant in the SEE. However, as we see in this section, most other molecules are found mainly in the CCS. The lines of all molecules analyzed in this section have several common features (see Figs. 2–5). The relatively small absorptions, when present, tell us that the emitters are not located too close to the continuum source. In addition these absorptions appear at velocities around -40 to -50 km s^{-1} , which do not correspond to the typical location of the absorption caused by gas in the SEE (around -29 km s^{-1} , see P04). Finally, the width of the emission is also the one expected for the velocities of the CCS. Therefore, the analysis of the lines from these molecules is quite simple following the method explained in § 3.

The calculations for most molecules in the cold circumstellar shell agree on a rotational temperature in this region around 30 K. This value is considerably lower than the 60 K considered in P05 to model $\text{HC}_{3,5}\text{N}$ lines in the ground or the lowest vibrationally excited states, probably due to the still large abundance of these species in zones between the SEE and CCS where the temperature has an intermediate value between ~ 263 and ~ 30 K.

4.1.1. H_2CO , SiO, and CS

The results for these three molecules agree on a rotational temperature around 25–30 K, similar to that found for other molecules present in the CCS. H_2CO (see also Cernicharo et al. 1989)

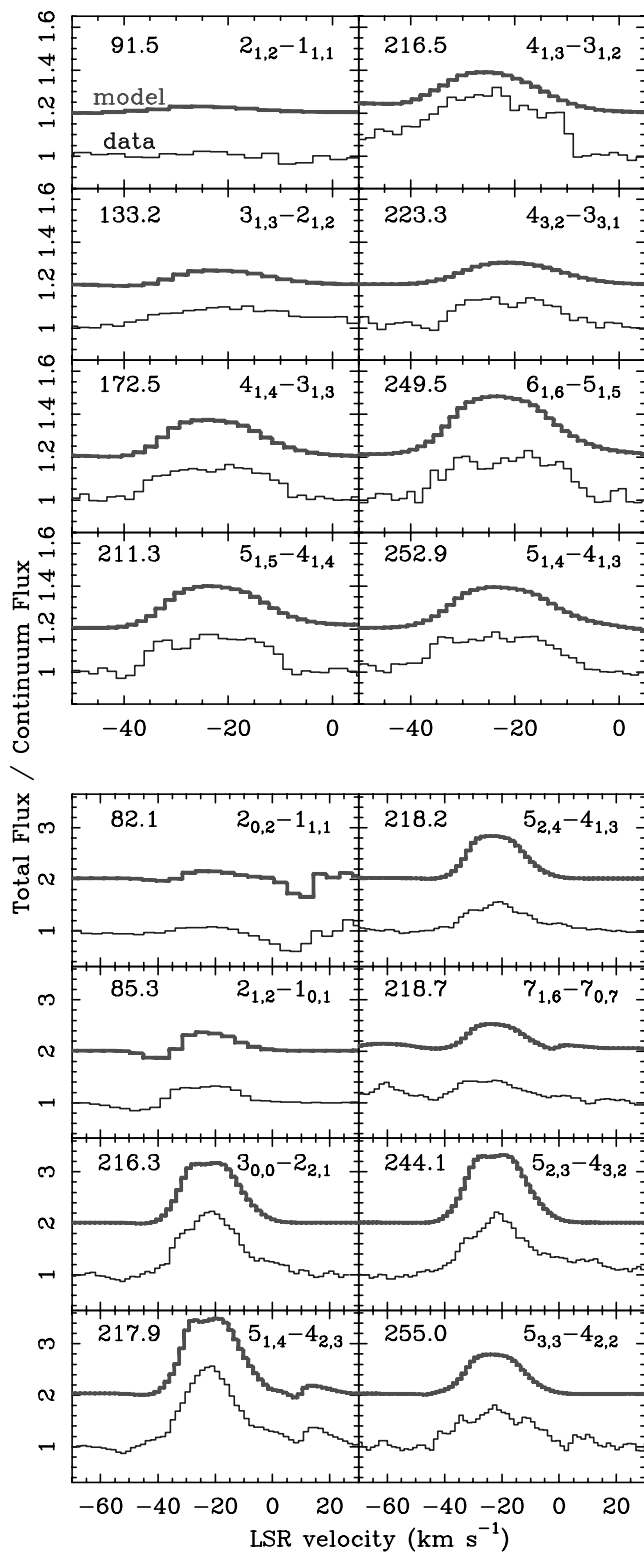


FIG. 3.—Data (not shifted) and best model (shifted by a different fraction of the continuum flux depending on the species) for the cyclic molecule C_3H_2 (bottom) and the cyclic radical C_3H (top) in CRL 618 (see § 4.1.2). We have indicated in each box the rotational numbers of the transition (top right corner) and the central frequency in GHz rounded to 0.1 GHz (top left corner). Nearby lines belonging to cyanopolyynes species are simulated according to P04 and P05. [See the electronic edition of the Journal for a color version of this figure.]

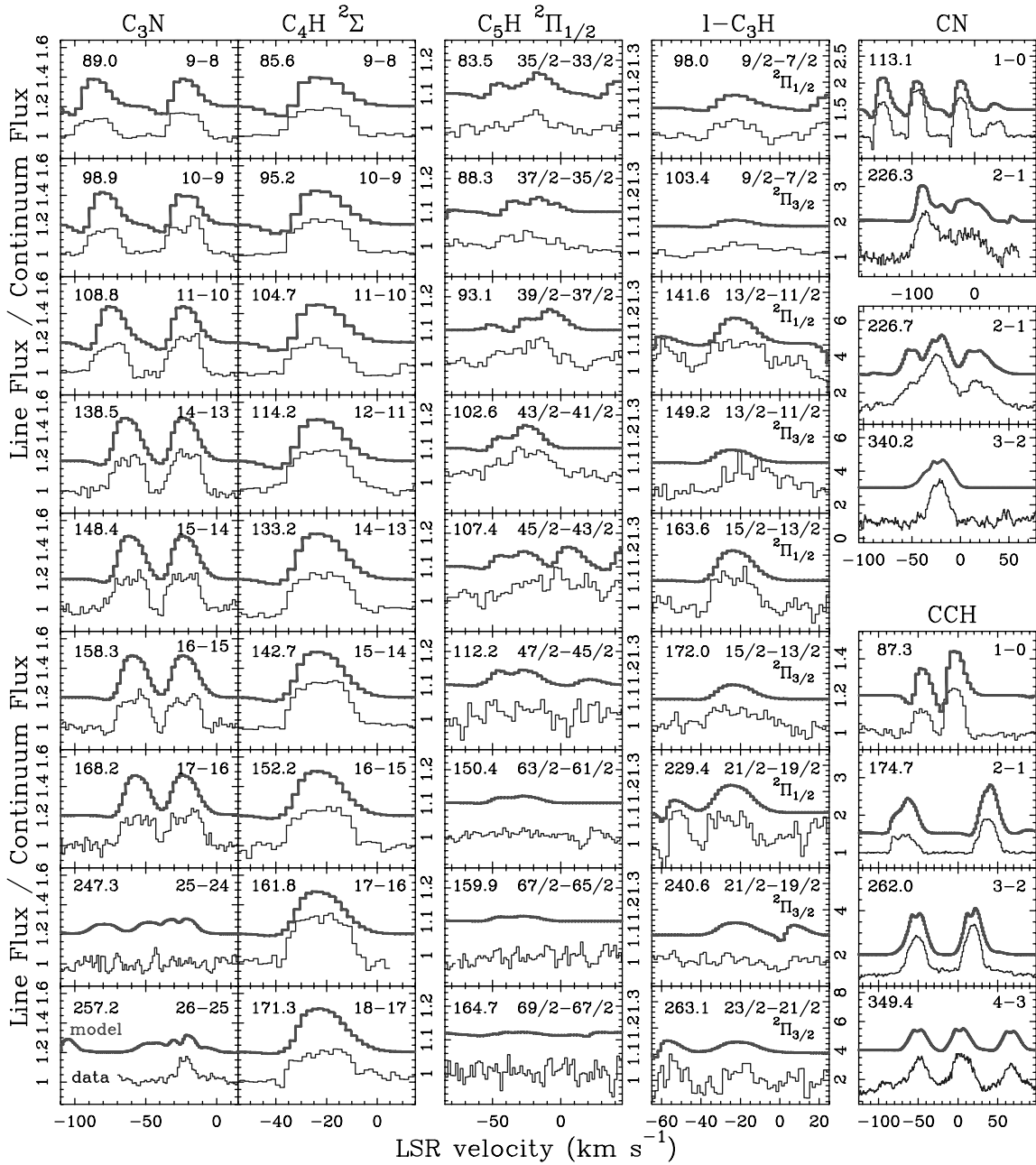


FIG. 4.—Data (not shifted) and best model (shifted by a different fraction of the continuum flux depending on the species) for linear radicals detected in CRL 618 (see § 4.1). We have indicated in each box the rotational numbers of the transition (top right corner) and the central frequency in GHz rounded to 0.1 GHz (top left corner). Nearby lines belonging to different species are simulated according to P04, P05, and this paper. [See the electronic edition of the *Journal* for a color version of this figure.]

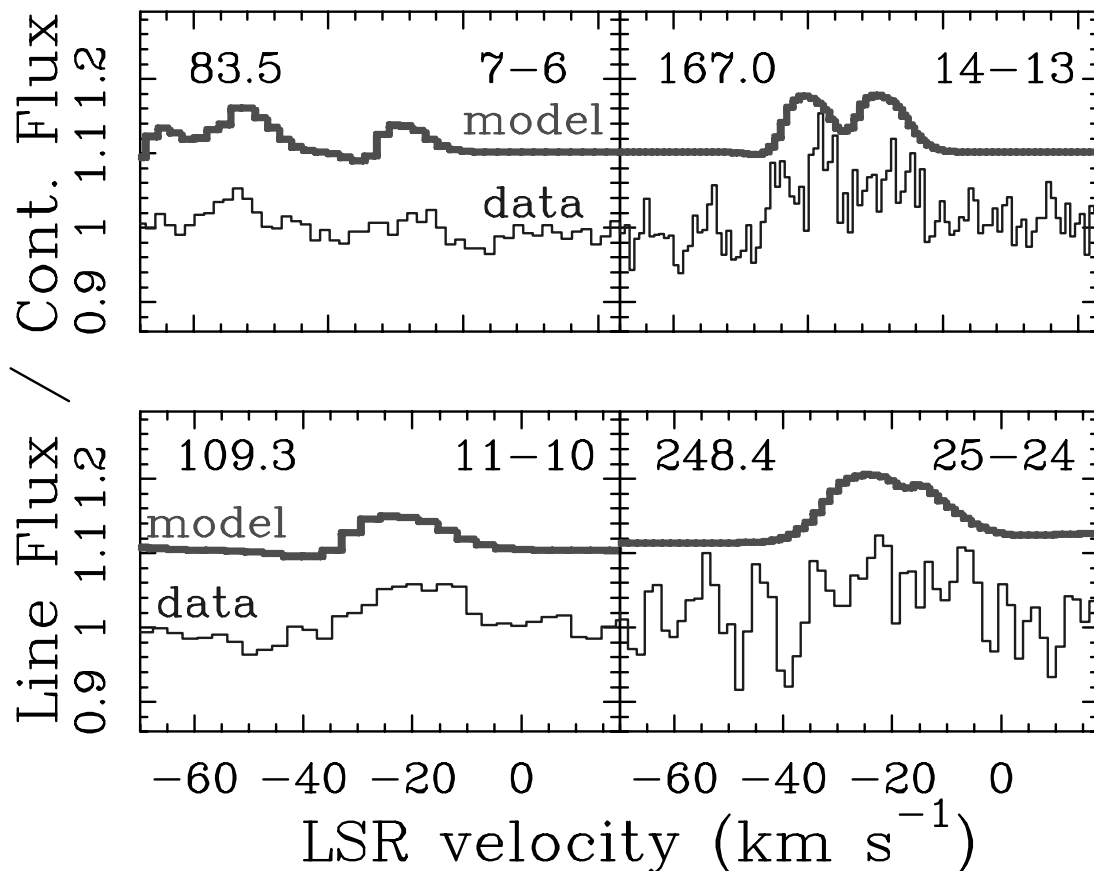


FIG. 5.—Data (not shifted) and best model (shifted by $0.1F_C$) for HCCNC and MgNC in CRL 618. Main quantum numbers ($J_{\text{up}}-J_{\text{low}}$) for each cluster of lines appear at the top right corner of each box. Reference frequencies rounded to 0.1 GHz appear at the top left corner of each box. These molecules are present only in the CCS with abundance ratios given in Table 2. [See the electronic edition of the *Journal* for a color version of this figure.]

and SiO are the only molecules with oxygen found in the survey in addition to CO and HCO^+ (§ 4.3). SiO is about 80 times less abundant than HC_3N in the CCS, whereas both CS and H_2CO are 10 times more abundant than SiO (inverse ratio with respect to HC_3N around 8). H_2CO exhibits several lines reaching peak fluxes of about half the continuum level, as well as CS, but the latter has only two lines suitable for analysis, and therefore, the results have larger uncertainties. It is interesting that the upper limit found for the ratio $[\text{HC}_3\text{N}]/[\text{H}_2^{13}\text{CO}]$ of ~ 300 would indicate a $^{12}\text{C}/^{13}\text{C}$ ratio over 40 in the CCS, to be compared with only ~ 15 in the SEE (P04). This lower limit for $^{12}\text{C}/^{13}\text{C}$ in the CCS is further supported by the nondetection of ^{13}CS and ^{13}C substituted species of HC_3N above the 3σ limit achieved in this survey (see P05). The implications of this result are discussed in § 4.4.

4.1.2. Cyclic Hydrocarbons

We have two cyclic hydrocarbons detected in the survey: the cyclic molecule C_3H_2 and the cyclic radical C_3H . All observational characteristics of their lines (line width, small or no absorption) indicate that they are both located in the CCS, like the radicals analyzed in 4.1.3. Their analysis has been very straightforward (see Figs. 1 and 3) and the results are very consistent. The fits provide the same rotational temperature for both (around 30 K), with C_3H_2 being a factor of ~ 3 less abundant than HC_3N , and $\text{c-C}_3\text{H}$ being ~ 7 times less abundant than C_3H_2 , consistent with a formation of $\text{c-C}_3\text{H}$ from C_3H_2 via photodissociation. The ^{13}C isotopic substitutions of both species could not be detected in the survey, indicating that a lower limit for the $^{12}\text{C}/^{13}\text{C}$ ratio is

~ 40 , providing further evidence of the result already pointed out in § 4.1.1 and discussed in § 4.4.

4.1.3. Linear Radicals

Although not reaching the wealth in long linear carbon chains and radicals found in IRC +10216 (Cernicharo et al. 2000), a series of linear radicals derived from cyanopolyynes species has been detected in CRL 618 (see Fig. 4). These radicals have large dipole moments, greater than 2 D except for C_4H (0.9 D), a fact that compensates somewhat their large partition functions for detection purposes. For example, C_5H , with a dipole moment of 4.88 D, has an estimated abundance in the CCS of ~ 200 less than HC_3N . Detections of C_6H and C_5N could not be confirmed. A rotational temperature of 30–35 K is again the one that provides the best fit for the whole group. Even the abundant CN and CCH radicals do not display evidences of their presence in the SEE, probably because there they would combine quickly with H_2 to give HCN and C_2H_2 due to the high volume density and temperature prevailing in this zone. Of special interest here is the large abundance of C_4H in the CCS (basically equal to that of HC_3N), a fact that has some parallelism with the high abundance of the same radical in IRC +10216 (Cernicharo et al. 2000). This large abundance allows us to also detect this molecule in the ν_7 state (about 30 weak features, not shown here, with rotational numbers up to $J = 22$). On the other hand, the linear C_3H radical displays weak lines, and the calculated abundance is a factor of 3 lower than its cyclic counterpart (see § 4.1.2). Finally, CN is about 1 order of magnitude more abundant than CCH in the CCS, just

opposite to the abundances of their combinations with a methyl radical (CH_3CN and CH_3CCH , see § 4.2). The analysis of ^{13}CN (detected), and ^{13}CCH and C^{13}CH (nondetected) confirms that $^{12}\text{C}/^{13}\text{C}$ is ~ 40 or larger in the CCS.

4.1.4. Other Molecules

We have also detected MgNC and the HC_3N isomer HCCNC fundamentally in the CCS (see Table 2 and Fig. 5). The detection of the isomer HNCCC could not be confirmed at the sensitivity level of the survey.

Another molecule detected in the survey is N_2H^+ . However, with only one line detected, the derived abundance ratio (~ 40 times less than HC_3N in the CCS) is uncertain.

4.2. Molecules Present Simultaneously in the SEE and the CCS

Apart from the cyanopolynes, we have found evidence of the simultaneous presence in the SEE and the CCS for the molecules CH_3CN and CH_3CCH . They are quasi-linear with clusters of lines separated by ~ 17 – 18 GHz. Both display similar intensities (see Fig. 6), indicating that $[\text{CH}_3\text{CCH}]/[\text{CH}_3\text{CN}]$ is of the order of $(\mu_{\text{CH}_3\text{CCH}}/\mu_{\text{CH}_3\text{CN}})^{-2}$ (~ 25). One interesting observational feature of the observed lines of both species is that there is very little absorption in the lowest observed CH_3CN transitions, and basically, an absence of them in higher transitions (see Fig. 6). In fact, the absorptions seen in the $J = 6-5$ and $J = 8-7$ spectra of CH_3CN are both actually due to HC_3N in the $3\nu_7$ vibrational state. The first interpretation of this fact would be that like for many other molecules or radicals analyzed in this paper (§ 4.1), the emission comes exclusively from the CCS. However, at the low temperatures of the CCS the line ratio between the different components of each cluster cannot be reproduced correctly. It turns out that the SEE component is also necessary to “activate” some components of the cluster, seen in the data, that arise from higher energy levels. The model to reproduce the observations of these molecules needs to simultaneously consider their presence in both the SEE and the CCS. Figure 6 illustrates the final model after this analysis. The resulting abundance ratios, considering rotational temperatures of 263 K in the SEE and 30 K in the CCS, appear in Table 3. According to these results, CH_3CCH is a molecule at least as abundant as HC_3N in the SEE, but due to its low dipole moment, the detection of ^{13}C substitutions is difficult at the sensitivity limit of the survey. A presence of these molecules in the HVW is also possible, according to the evidence of wings especially for groups of lines above 200 GHz. More complex molecules of this family, such as CH_3CCCN , cannot be seen.

4.3. Abundant and More Extended Molecules

In addition to HC_3N , the most abundant molecules in CRL 618 are CO , HCN , HNC , and HCO^+ . However, contrary to HC_3N , these molecules have very small partition functions, and their lines detected in the survey involve very low energy levels. As a result, the lines from the main isotopomers are usually optically thick. From the peak emission it can then be derived that these molecules are more extended than most other species (see the case of HCN and HCO^+ in Sánchez-Contreras & Sahai 2004). For example, for CO if we consider the lines as optically thick and coming only from inside the outer radius of the CCS defined in our model, the observed peak line flux, predicted from the coupling to the telescope beam, would be too small. If we allow CO to emit in a more extended region, the model can predict quite correctly the peak of the lines (see Fig. 7). The result found (outer diameter of CO -emitting region, at 30 K, of about $17''$) is quite consistent because it provides a very good fit to three different lines observed with

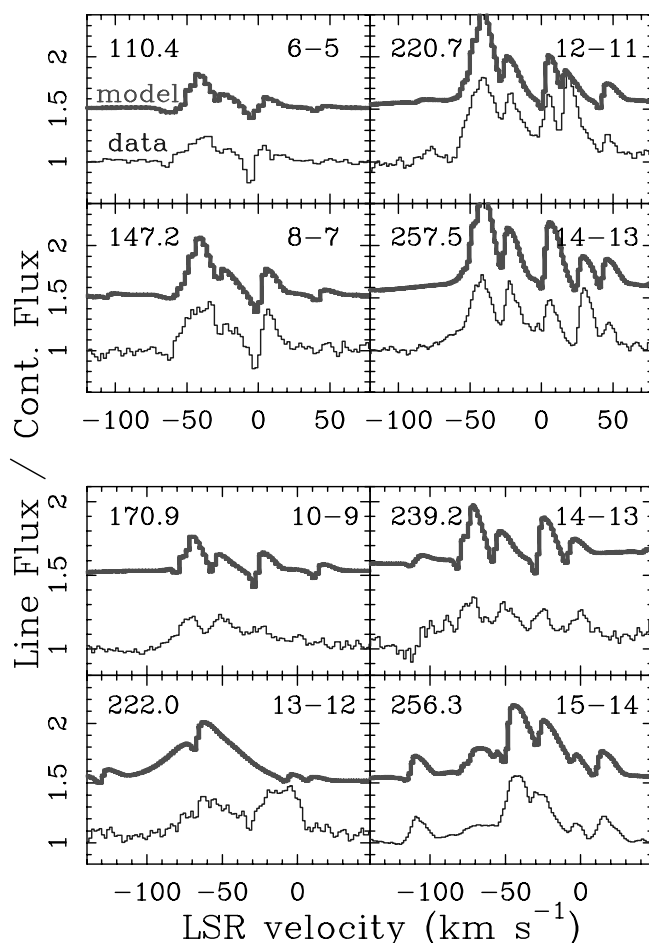


FIG. 6.—Data (not shifted) and best model (shifted by $0.5F_C$) for CH_3CN and CH_3CCH in CRL 618. Main quantum numbers ($J_{\text{up}}-J_{\text{low}}$) for each cluster of lines appear at the top right corner of each box. Reference frequencies rounded to 0.1 GHz appear at the top left corner of each box. The line centered at ~ 10 km s^{-1} in the 222 GHz panel of CH_3CCH is one of the strongest unidentified features of the survey at present. The line flux of the $J = 15-14$ cluster of CH_3CCH has been divided by 4 for both data and model in order to keep the same scale. As discussed in § 4.2, to reproduce the data, we need to consider that both molecules are present in the SEE and the CCS (and possibly in the HVW) (see Table 3). [See the electronic edition of the Journal for a color version of this figure.]

two different telescopes ($J = 1-0$ and $J = 2-1$ at the IRAM 30 m, and $J = 3-2$ at the CSO). Another interesting fact is that the emission in the form of broad wings arising from the HVW region, seen in all four molecules, is not optically thick, and therefore, we can determine abundances with respect to HC_3N in the HVW quite well. The absorption feature (against the HWV component) centered at ~ -55 km s^{-1} in ^{12}CO $J = 1-0$, which disappears in higher transitions, can provide some constraints about the CO column density in the CCS, and the same is valid for the other three molecules. The lines from ^{13}C isotopic substitutions (and also from C^{17}O and C^{18}O in the case of CO) are not saturated (with the exception probably of ^{13}CO) and, therefore, provide a good abundance estimate in the CCS that can be combined with the $^{12}\text{C}/^{13}\text{C}$ value derived earlier in the paper (~ 40) and discussed in detail in § 4.4 in order to check the consistency of the values assumed for the main isotopomers. Finally, lines from vibrationally excited states (such as $\text{HCN } \nu_2$ in the red wing of HCN $J = 2-1$ and $J = 3-2$) arise mainly from the SEE at frequencies where they can be seen and, therefore, allow us to constrain the HCN abundance there too. For the $J = 1-0$ transition of both HNC and HCO^+ , it looks like the CCS is partially transparent, so

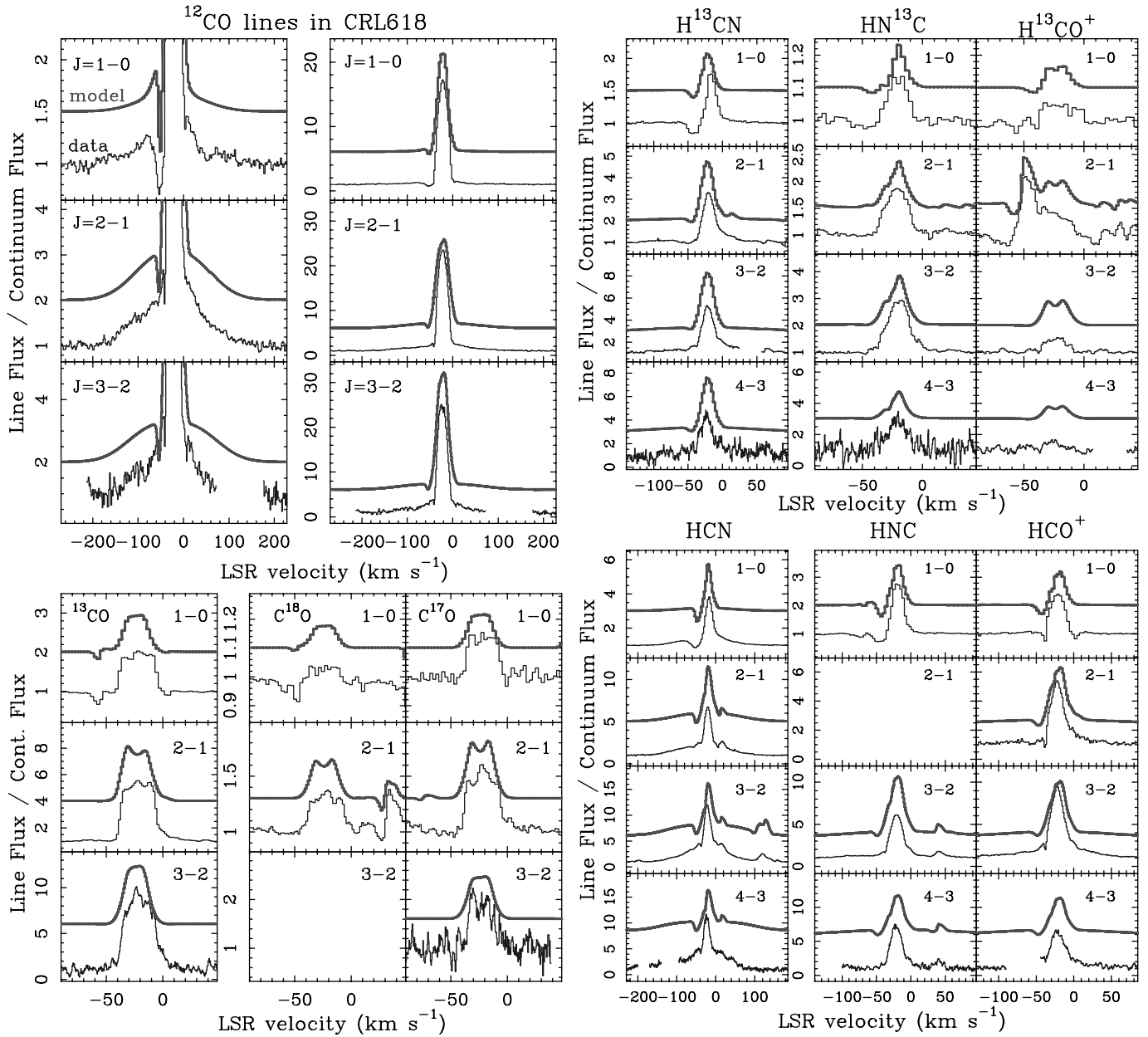


FIG. 7.—Strongest lines found in the 80–360 GHz survey of CRL 618 (first rotational lines of CO, HCN, HNC, and HCO^+), and their counterparts for different isotopomers. The lines of the main species usually reach saturation and therefore the peak values allow us to derive the size of the emitting region if a given rotational temperature is assumed. See Table 3 and § 4.3. The resulting model is shifted with respect to the data by different amounts depending on the species and transition. The lines from ^{13}CO , C^{17}O , and C^{18}O are not saturated and give a useful value of the abundance of these isotopomers in the CCS (see Table 3). All lines have been observed with the IRAM 30 m telescope except the 3–2 transition of CO and its isotopomers, and the 4–3 transition of HCN, H^{13}CN , HNC, HN^{13}C , HCO^+ , and H^{13}CO^+ (all these observed with the CSO, with image sideband artifacts removed). Note the consistency of the model for a series of lines observed with two different telescopes working at different frequencies and having quite different apertures, once the proper source coupling is applied. [See the electronic edition of the Journal for a color version of this figure.]

that some information of the SEE can also be obtained. Using all these tools, the abundances of CO, HCN, HNC, and HCO^+ , and the extension of their emission, have been determined (see Table 3), providing a quite consistent model for all their lines (see Fig. 7). We should remark that this solution is quite well constrained. Other sizes for the emitting region would result in wrong peak levels for species with optically thick lines. Other abundance ratios of the main isotopomers with respect to ^{13}C substituted species (not following the $^{12}\text{C}/^{13}\text{C}$ ratios derived earlier in this study) would result in a poorer reproduction of the absorption features produced by the CCS gas against the continuum and/or the HVW component.

The fact that for all species analyzed in this section two different telescopes have been used (meaning different couplings to the source) with consistent model results also reinforces our results.

4.4. $^{12}\text{C}/^{13}\text{C}$ Ratios in the SEE and the CCS

One result of this study (see §§ 4.1.1 and 4.1.2) that can be surprising is the different $^{12}\text{C}/^{13}\text{C}$ ratios in the SEE and the CCS. In this section we propose an extra check of this result by looking at the rotational lines from $v = 0$ in HC_3N , HC^{13}CCN , HCC^{13}CN , $\text{H}^{13}\text{C}^{13}\text{CCN}$, and $\text{H}^{13}\text{CC}^{13}\text{CN}$. The explored energy range (~ 21 – 293 K) allows us to easily distinguish one region from the other

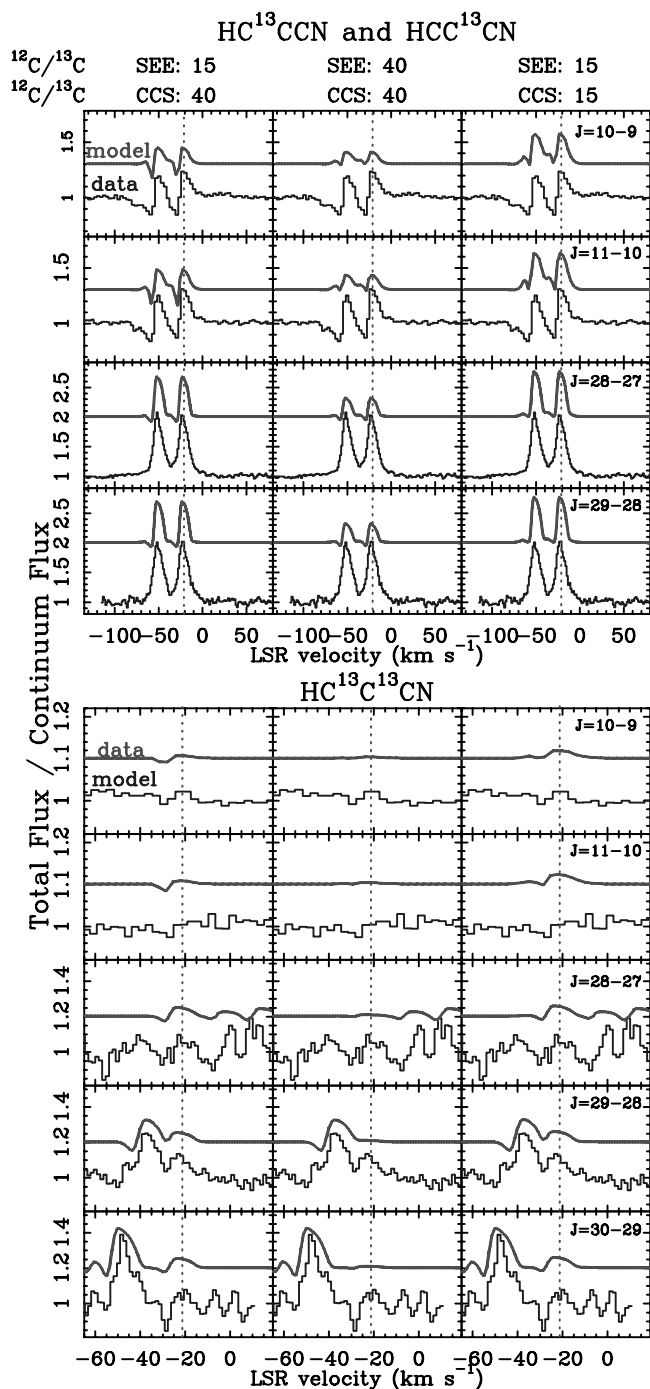


FIG. 8.—Simulations and data of selected lines of isotopic HC_3N in the ground vibrational state to find the value of $^{12}\text{C}/^{13}\text{C}$ in the SEE and the CCS of CRL 618. [See the electronic edition of the *Journal* for a color version of this figure.]

with a proper selection of lines. Figure 8 shows the predictions for a sample of lines of these molecules with different values of the $^{12}\text{C}/^{13}\text{C}$ ratios in the SEE and the CCS, from which we can see that the values used in this work (15 in the SEE and 40 in the CCS) give the best results. According to this figure, the value $^{12}\text{C}/^{13}\text{C} = 15$ in the SEE is the one that is more clearly determined, because the 1 mm lines (mostly originated in the SEE) of the single ^{13}C -substituted HC_3N would appear too weak if that value was around 40. Further evidence of this result was already provided in P05 by studying rotational lines within the ν_7 vibra-

tional state of single ^{13}C -substituted HC_3N (see their § 4.2 and Fig. 2). Finally, the obtained detection of doubly ^{13}C -substituted HC_3N at 1 mm is only possible with the value ~ 15 . On the other hand, evidence for $^{12}\text{C}/^{13}\text{C} \sim 40$ in the CCS is found in the 3 mm lines of the single ^{13}C -substituted HC_3N (T_{ex} similar to the temperatures of this region), because if that value was around 15, the observed absorption would disappear. Additional evidence is provided by ^{13}CS , H_2^{13}CO , ^{13}CCH , C^{13}CH , etc. Because of the wealth of lines available for this analysis, the error bars on the $^{12}\text{C}/^{13}\text{C}$ values found for the SEE and the CCS are less than 10%. Our result in the SEE is in relative good agreement with the one found by Wyrowski et al. 2003 ($^{12}\text{C}/^{13}\text{C} = 10 \pm 2$).

Some objects evolving to the planetary nebula phase show evidence of low $^{12}\text{C}/^{13}\text{C}$ ratios in the gas surrounding the central star. One example is V4334 Sgr, in which the $^{12}\text{C}/^{13}\text{C}$ ratio in the gas seems to be around 4 (Asplund et al. 1999; Pavlenko et al. 2004). The one thing that is of particular interest in CRL 618 is that we have evidence of two distinct gas regions with clearly different values of $^{12}\text{C}/^{13}\text{C}$, and this may indicate injection of ^{13}C -rich material to the gas surrounding the central star. The $^{12}\text{C}/^{13}\text{C}$ value in the CCS (~ 40) can be considered similar to that of the solar system (~ 70), but obviously, ^{13}C appears to be overabundant in the inner SEE. As in the case of V4334 Sgr, the origin of the ^{13}C -rich material may be found in a late CNO cycling phase that follows the He burning phase in which the ^{13}C abundance should be closer to the solar system value. In fact, the $^{12}\text{C}/^{13}\text{C}$ equilibrium value from CNO cycling is ~ 3.5 (Asplund et al. 1999), and therefore, we can imagine that the ^{13}C -rich material is being injected to the SEE of CRL 618 right now. The injection of this material has not yet reached the outer gas regions, thus explaining the higher (and more consistent with He-burning) $^{12}\text{C}/^{13}\text{C}$ in the CCS.

5. SUMMARY AND FUTURE WORK

Using a proper selection of lines (usually around 8) for the different molecular species detected in the 80–276 GHz line survey of CRL 618, their abundances and location in this object have been derived with much better accuracy and completeness than any earlier work thanks to the amount of data and their consistent calibration. An overabundance of ^{13}C has been noticed in the inner gas regions, probably due to injection of ^{13}C -rich material resulting from CNO cycling in the central star. The results of the analysis are summarized in Tables 2 and 3. These, together with those already presented in P04 and P05, provide the most complete picture of the physical conditions and chemical structure of the gas envelopes of CRL 618. They also allow us to run a model of the whole millimeter-wave spectrum of CRL 618 to be compared with the line survey in order to check the consistency of the whole study.

Comparison of data and model ease the task of isolating U lines and detecting calibration problems in some spectra. In the next and final paper of this series we will present the whole IRAM 30 m survey of CRL 618 with the most complete line identification up to date and the full detailed comparison of data and model.

We thank the support of the IRAM 30 m staff during the long completion of the line survey. CSO operations are supported by US NSF grant AST 02-29008. This work has been supported by Spanish grants AYA2003-02785 (National Administration) and S-0505 ESP-0237 (Madrid Region Administration).

REFERENCES

- Asplund, M., Lambert, D. L., Kipper, T., Pollacco, D., & Shetrone, M. D. 1999, *A&A*, 343, 507
- Cernicharo, J. 2004, *ApJ*, 608, L41
- Cernicharo, J., Guélin, M., & Kahane, C. 2000, *A&AS*, 142, 181
- Cernicharo, J., Guélin, M., Peñalver, J., Martín-Pintado, J., & Mauersberger, R. 1989, *A&A*, 222, L1
- Pardo, J. R., Cernicharo, J., & Goicoechea, J. R. 2005, *ApJ*, 628, 275 (P05)
- Pardo, J. R., Cernicharo, J., Goicoechea, J. R., & Phillips, T. G. 2004, *ApJ*, 615, 495 (P04)
- Pavlenko, Ya. V., Geballe, T. R., Evans, A., Smalley, B., Eyres, S. P. S., Tyne, V. H., & Yakovina, L. A. 2004, *A&A*, 417, L39
- Sánchez-Contreras, C., & Sahai, R. 2004, *ApJ*, 602, 960
- Williams, D. 2003, *Astron. Geophys.*, 44, 14
- Wyrowski, F., Schilke, P., Thorwirth, S., Menten, K. M., & Winnewisser, G. 2003, *ApJ*, 586, 344